Harris functional densities: from solid to atom

1996 J. Phys.: Condens. Matter 8 7379

(http://iopscience.iop.org/0953-8984/8/40/005)

J. Phys.: Condens. Matter **8** (1996) 7379–7391. Printed in the UK

Harris functional densities: from solid to atom

J Hartford, L B Hansen† and B I Lundqvist

Department of Applied Physics, Chalmers University of Technology and Göteborg University, S-412 96 Göteborg, Sweden

Received 29 March 1996, in final form 9 July 1996

Abstract. Adaptive and transferable electron densities applicable as input in Harris density functionals and first-principles inter-atomic potentials are constructed from calculations for the atom in question embedded in a homogeneous electron gas. The density profile of each atom depends explicitly on the average density in which the atom is located, which forms the basis for the adaptivity. Harris functional results for Al and Ni atoms in numerous configurations are compared to the corresponding self-consistent results. The new density construction is shown to give systematically better results than superimposed fixed atom-like densities.

1. Introduction

Self-consistent (SC) total-energy calculations based on density functional theory (DFT) have become extremely useful as tools for investigating the energetics and dynamics of solids [1–3]. In principle, total energies of any system can be calculated with only atomic numbers as input. In practice, the necessity of repeatedly solving the Schrödinger and Poisson equations until self-consistency is achieved, involving many numbers to represent the electron density and potential, set severe restrictions on the size of the systems amenable to study.

Alternative schemes for eliminating the time-consuming self-consistency cycle or for simplifying descriptions of the density and potential are consequently of great importance. Compared to the Hohenberg–Kohn–Sham (HKS) functional, the Harris (H) functional [4, 5] is a DFT functional that does not require the construction and solution of Poisson's equation for the output density. It has been found to have a smaller error for deviations from the ground-state density compared to the HKS functional [6, 7]. This property of the H functional makes it ideal for use in SC as well as non-SC methods. The application of the non-SC H functional requires a good, i.e. transferable and physically sound, input density that can be used in different atomic environments.

The obvious first choice is that obtained by superimposing free-atom charge densities. Applications have been made with this prescription on a variety of systems: molecules, metals, semiconductors, and even ionic crystals [4, 8, 9]. It has been shown that superimposed free-atom densities work well for properties of the perfect lattice but not for defect structures, such as surfaces and vacancies [6, 7].

To improve on an atom-like density mainly two paths are possible: (i) a restricted iterative search aiming at coming closer to the SC solution [10–13]; or (ii) a 'one-shot' calculation with some optimized input density [14, 15]. We follow the latter path in this paper and test the applicability of embedding densities in the Harris functional. Such optimized densities can also be utilized for tight-binding (TB) constructions [16].

† Present address: CAMP, Physics Department, Technical University of Denmark, DK-2800 Lyngby, Denmark.

0953-8984/96/407379+13$19.50

The above-mentioned surface problem has been addressed by several authors. Finnis [7] resolved the problem by using a two-parameter variation of the input density to reproduce the surface energy. Later Chetty *et al* [14] and Robertson *et al* [15] constructed an optimized density by fitting the density in reciprocal space to the points from SC calculations for both surface and bulk configurations, exploiting the fact that the surface and bulk systems give density contributions that are effectively separated in reciprocal space.

The present work provides a real-space method, treating each atom separately in a way that allows adaptive atom-like densities. It accounts for the differences in surroundings that each atom can experience (i.e. effective coordination) by using induced densities for the atom considered embedded in homogeneous electron gases (jellia) at varying densities. In this way one can obtain a renormalized-atom-like density that gradually changes as its environment changes. Our construction is flexible enough to apply from bulk systems to free atoms. The atom-in-jellium model is known to account well for trends of bulk properties, such as inter-atomic distances, cohesive energies, and compressibilities [19, 20]. In bonding systems, electronic screening causes a contraction of the atomic density tail. The embedding provides a physical method for obtaining such a renormalized density.

An important aspect of the H functional is the fact that it provides a basis for first-principles inter-atomic potentials of TB type [16, 17] and for schemes with a relaxed degree of self-consistency [10–13, 18]. The H functional with a transferable density can thus be viewed as the basic approximation behind glue schemes, such as the effective-medium theory (EMT) [20] and the embedded-atom method (EAM) [21]. Our approach follows the idea of the original implementation of the EMT by Jacobsen *et al* [20], in which the parametrization of the atomic density explicitly depends on the average density of the surrounding atoms at the atomic site. So far, however, the idea has not been tested in real solid-state surroundings, using an accurate functional, such as the Harris functional, used in this work.

We apply our input densities to a broad range of structures, including uncoordinated free atoms, low-coordinated surfaces and high-coordinated bulk ones. Our density construction is found to give H energy values closer to the SC results than what would be given with a single atom-like density. We credit the systematically better agreement for total energies and density distributions, in particular at low coordinations, to its adaptivity, accounting for the density variations of the surrounding media. In fact, this approach comes very close to the limit of accuracy possible with the H functional that can be obtained with superimposed spherical densities. Robertson *et al* [15] have reported this limit, set by the inability to describe properties that ultimately depends on non-symmetric charge redistributions, to be 0.02–0.03 eV per atom for Al.

In the next section we discuss the Harris functional and some of its properties. The method for obtaining the Harris input densities from embedding calculations is presented in section 3. In section 4 we give total energies in the local density approximation (LDA) [22] for the new densities, the density derived by Finnis and the SC results. Finally, in section 5 we draw conclusions and discuss further applications.

2. The Harris functional

In self-consistent DFT one solves the many-body electron problem by minimization of the HKS total-energy functional [1, 22]:

$$E^{\mathrm{HKS}}[n^{\mathrm{out}}(\boldsymbol{r})] = \sum_i f_i^{\mathrm{out}}\epsilon_i^{\mathrm{out}} - \int \mathrm{d}^3r\; n^{\mathrm{out}}(\boldsymbol{r})\left(\Phi[n^{\mathrm{in}}(\boldsymbol{r})] - \frac{1}{2}\Phi[n^{\mathrm{out}}(\boldsymbol{r})] + v_{\mathrm{xc}}[n^{\mathrm{out}}(\boldsymbol{r})]\right)$$

$$+ E_{\rm xc}[n^{\rm out}(\boldsymbol{r})] + E_{\rm ion} \tag{1}$$

with well known terms: one-electron energy eigenvalues ($\epsilon_i^{\rm out}$), Coulomb (Φ) and exchange–correlation ($v_{\rm xc}$) potentials, exchange–correlation energy ($E_{\rm xc}$) and ionic energy ($E_{\rm ion}$). The minimum is found by iterating the Kohn–Sham equations until self-consistency is achieved, i.e. when $n^{\rm out}$ equals $n^{\rm in}$. For large systems this is very time consuming and one possibility for decreasing the computational effort is to start with a good trial density ($n^{\rm in}(\boldsymbol{r})$) and just take one step in the iteration. We will refer to this approach as the non-self-consistent HKS functional (which will depend on the output density, $n^{\rm out}(\boldsymbol{r})$, of the step). The HKS functional is a variational upper bound to the SC energy.

The alternative functional proposed by Harris is quite similar [4, 5]. However, it does not depend on the output density of the iterative step in the Kohn–Sham equations and therefore there is need neither for construction of the output density nor for the solution of Poisson's equation. This is a great advantage to methods using atom-centred basis sets. We may write it as

$$E^{\rm H}[n^{\rm in}(\boldsymbol{r})] = \sum_i f_i^{\rm out}\epsilon_i^{\rm out} - \int {\rm d}^3r\; n^{\rm in}(\boldsymbol{r})\left(\frac{1}{2}\Phi[n^{\rm in}(\boldsymbol{r})] + v_{\rm xc}[n^{\rm in}(\boldsymbol{r})]\right) + E_{\rm xc}[n^{\rm in}(\boldsymbol{r})] + E_{\rm ion}. \tag{2}$$

The H and HKS functionals are of course identical when $n^{\rm in} = n^{\rm sc}$, but for deviations of $n^{\rm in}$ from $n^{\rm sc}$ the two functionals behave differently. The error caused by $n^{\rm in} \neq n^{\rm sc}$ is in general larger for the HKS functional because there is a considerable 'overshooting' in the output density resulting in mainly Coulomb energy errors [7]. Using a jellium model combined with the Thomas–Fermi approximation for the density response function, the error for a specific extended system has been found to be given by [6]

$$\begin{aligned} E^{\rm HKS}[n^{\rm in}] - E[n^{\rm sc}] &= \mathcal{O}[(n^{\rm in} - n^{\rm sc})^2/q_0^4] + \text{higher-order terms} \\ E^{\rm H}[n^{\rm in}] - E[n^{\rm sc}] &= -\mathcal{O}[(n^{\rm in} - n^{\rm sc})^2/q_0^2] + \text{higher-order terms.} \end{aligned} \tag{3}$$

Here q_0 is a characteristic reciprocal wavevector. Equation (3) implies that for both functionals the Coulomb energy errors dominate for systems containing small wavevectors, like surfaces, and this has been extensively reported [6, 7, 14, 15].

The results in equation (3) suggest that the H functional should have a maximum at the SC density, but it has been shown that the extremum is either a local minimum or a saddle point (in the LDA it is a saddle point) [23]. When the characteristic reciprocal wavevector is below a certain critical value, the Coulomb energy dominates and the functional behaves as if it has a local maximum [23]. For a general system, however, it is not possible to find upper and lower bounds to the total energy by calculating HKS and H energies. In section 4 we find for the Al surface system saddle-point behaviour of the functional.

3. Construction of overlapping embedding densities

3.1. Atoms embedded in jellium

An atom embedded in a homogeneous electron gas ('jellium') is a model system for solids that has appealed to many theorists over the years. In this approach one focuses on a single atom and examines its interaction with a host of extended states.

Each atom of the collection that a solid consists of feels and responds to an environment. The latter may be considered in some approximate way, particularly in simple metals because of efficient electronic screening. Probably this line of thinking started with the study by

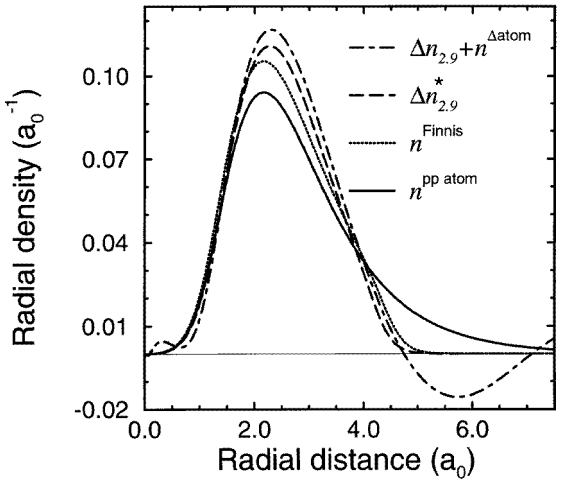

Figure 1. The Al-induced embedding valence density ($\Delta n_{2.9} + n^{\Delta atom}$) with the neutral radius $s = 2.9$ and a fit ($\Delta n^{*}_{2.9}$) using equation (A1). The empirical Finnis construction, quite alike our embedding density, is included for comparison. The most pronounced effect, relative to the case of the free pseudopotential atom, is the contraction of the density tail. It is seen that the valence full-electron density is fairly close to that of the pseudopotential atom inside the pseudo-core (which has a radius of about $2.5\,a_0$).

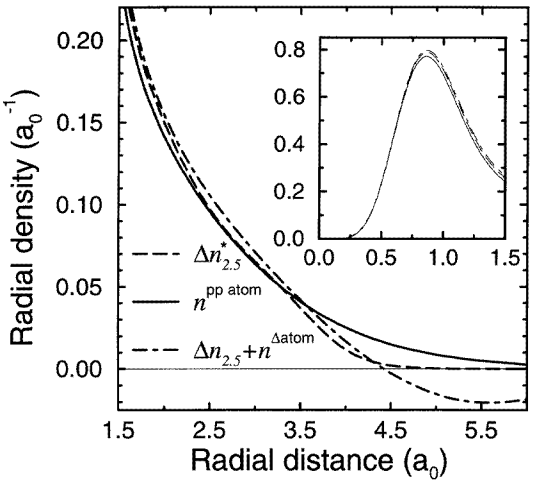

Figure 2. The Ni-induced embedding valence density ($\Delta n_{2.5} + n^{\Delta atom}$) with the neutral radius $s = 2.5$ and a fit ($\Delta n^{*}_{2.5}$) using equation (A2). The pseudopotential atom density is included for comparison. The inset shows the inner part of the densities. The pseudopotential core radius is about $2\,a_0$.

Wigner and Seitz of the cohesion of alkali metals [24]. It then reappeared in such models as cellular methods [25], spherical solids [26], the renormalized-atom model [27, 28], the atom-in-jellium model [19], and the EMT [20].

A key quantity is the density distribution, $n(r)$, of the immersed atom, calculated as a function of the background density, $\bar{n}$. The neutral-sphere radius, s, of an embedded atom

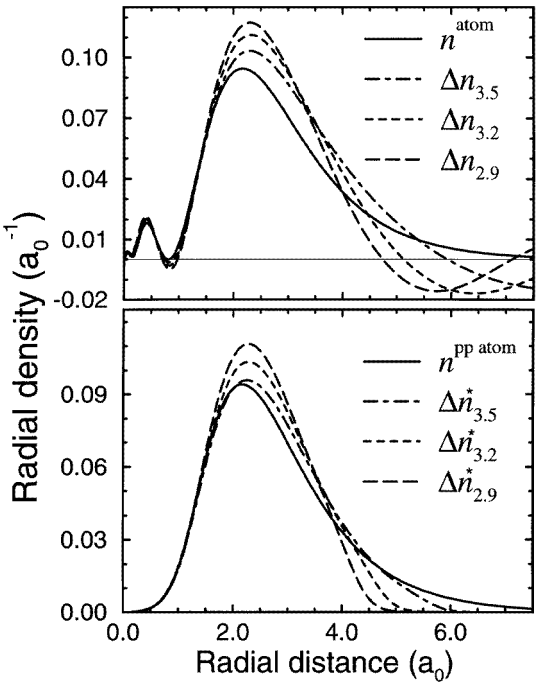

Figure 3. The upper panel shows valence embedding densities (Δn_s) for Al for several embedding background densities, and fits with equation (A1) to these are shown in the lower panel (Δn_s^*). The range of the fitted densities (used in the H calculations) is chosen to be determined by the beginning of the Friedel oscillation. The figure also illustrates the dependence of the density tail on the embedding background.

is simply related to this background density [20]. The induced density due to the atom is defined by subtracting the background:

$$\Delta n_s(r) = n_s(r) - \bar{n}_s.$$

Examples for Al and Ni calculated in the LDA are given in figures 1 and 2, respectively.

When using this density in the HKS and H functionals, we face two practical problems. One is connected with the use of a pseudopotential total-energy program. The *full-electron* density $\Delta n_s(r)$ is therefore converted by adding the difference between the densities of the free pseudopotential atom (pp atom) and the free full-electron atom, $n^{\Delta\text{atom}} = n^{\text{pp atom}} - n^{\text{atom}}$, to the induced densities.

The other problem is due to the Friedel oscillations in the induced density. Mere use of overlapping induced densities would give regions with negative total density, e.g. at surfaces. To solve this problem the induced density is forced into a non-negative functional form. We do this in two steps: first we fit a smooth positive function—see the appendix—to $\Delta n_s(r) + n^{\Delta\text{atom}}$ and then we normalize the total charge with $1/(1 + (r/r_0)^2)$, to obtain our pseudopotential-induced density, $\Delta n_s^*(r)$, hereafter just called the induced density. The procedure results in densities which are close to the original ones inside the neutrality radius, where the embedding density generally should be close to the SC density of a highly coordinated atom. The region outside the neutral radius is the critical part and the results depend quite strongly on the chosen range of the density tail. We have chosen to let the effective range of the renormalized atom be determined by the beginning of the

Friedel oscillation where $\Delta n_s(r)$ goes negative; see figure 1. In the limit of large s (low coordination), the free atom is retained from $\Delta n_s^*(r)$.

Figure 3 shows densities with increasing neutral radii illustrating the transition from compact bulk-like density to long-ranged free-atom density. Examination of the Al density decomposed with respect to angular momentum shows s-to-p promotion and a contraction of mainly p orbitals, which result in an increase and an outward push of the valence density peak. Aluminium constitutes the test case for our proposed density construction and will be discussed extensively in section 4.

The d electrons of Ni are to a large extent located inside the pseudopotential core radius (see figure 2) and the validity of merely adding the difference between free-atom densities is not obvious and we restrict this first study of Ni to just a single density. Comparison of the atomic and induced densities shows a rearrangement from s to mainly d but also p states. The d orbitals are contracted and the p states contribute to the outward push of the valence peak. It is noteworthy that the induced density cannot be reproduced by just rearranging the occupation of atomic orbitals.

No doubt our generation of induced densities can be made more straightforward, by using either the pseudopotential in the embedding program or an all-electron total-energy functional. However, this does not affect our key points.

Table 1. Radii of neutral spheres according to equation (4) for Al ions in the structures used for calculations.

	Neutral-sphere radii (a_0) for		
Structure	bulk atoms	surface atoms	adatoms
fcc, $a = 7.48\ a_0$	2.9	—	—
fcc, $a = 7.75\ a_0$	3.0	—	—
111 adatom:			
$z = 3.59\ a_0$	3.0	3.0	3.11
$z = 3.76\ a_0$	3.0	3.05	3.15
$z = 4.04\ a_0$	3.0	3.12	3.22
$z = 4.37\ a_0$	3.0	3.12	3.31
$z = 5.05\ a_0$	3.0	3.12	3.48
111 vacancy:	3.1	3.22	—
111 slab	3.0	3.09	—
100 slab	3.0	3.12	—
110 slab	3.0	3.16	—

3.2. Neutral spheres

As mentioned in the introduction, the induced density used as an input to the H functional should be flexible enough to be used in different atomic environments, which we assume can be described by an effective coordination number. The mechanism to account for this effective coordination number is provided by allowing the induced density $\Delta n_s^*(r)$ to depend on the background density of the electron gas in the embedding calculation and on s, the neutral-sphere radius. This sphere, inside which the total charge of the nucleus and electrons vanishes, varies in size with the environment. Just as in the EMT and effective-medium tight-binding (EMTB) model [20, 16] the neutral radii of atoms in arbitrary structures are calculated by integrating the induced densities of the atom itself and of its surrounding neighbours. For a system of atoms this gives a set of non-linear equations, which are easily

solved to a reasonable accuracy. For each atom this gives an s-value, and from that an induced density, $\Delta n_s^*(r)$. Assigning radii in an fcc crystal with the SC equilibrium lattice constant according to the above, we obtain for Al $s = 2.9\,a_0$ and for Ni $s = 2.54\,a_0$, corresponding to $\bar{n} = 0.008\,84\,a_0^{-3}$ and $\bar{n} = 0.0115\,a_0^{-3}$, respectively. The LDA lattice constants are for Al $7.48\,a_0$ and for Ni $6.56\,a_0$, and to within 1% we have neutral radii equal to the Wigner–Seitz radii.

In low-symmetry situations we have found reasons to modify the above original model. The neutral radius of, e.g., a surface adatom is fairly large, and the corresponding induced density placed at the ion position will have a long tail into the surface. We try to compensate for this asymmetry by using an effective neutral radius for the assignment of the induced density. We define this effective radius to be the average over the neutral radii for the atom i and of its overlapping nearest neighbours with neutral radii s_j:

$$s_i^{\mathrm{av}} = \left(\left\langle \sum_{j=\mathrm{n.n.}} s_j \right\rangle + s_i\right)\Big/ 2. \tag{4}$$

Radii calculated according to equation (4) differ from the neutral radii in having very asymmetric structures, like surfaces and surfaces with adatoms, but are essentially the same in bulk systems. The new radii for our Al structures are presented in table 1.

Our input density to be used in H and HKS functionals is the superimposed sum

$$n^{\mathrm{in}}(\boldsymbol{r}) = \sum_{\boldsymbol{R}_i} \Delta n^*_{s_i^{\mathrm{av}}}(\boldsymbol{r} - \boldsymbol{R}_i) \tag{5}$$

where $\boldsymbol{R}_i$ is the lattice positions of the ions.

4. Total-energy calculations for surfaces

In this section we test the construction of the density for various surface problems. In all calculations we use an LDA pseudopotential plane-wave code (DACAPO [29] and CASTEP [30, 31]), with norm-conserving pseudopotentials for Al and Ni [32, 33]. The cut-offs for the plane-wave basis sets used for Al and Ni are 150 eV and 1000 eV, respectively.

Table 2 shows the results for Al, obtained using four different kinds of superimposed input density: (i) the induced embedding density for the equilibrium fcc structure ($a = 7.48\,a_0$), $\Delta n_{2.9}$; (ii) a density Δn_s^* that depends on the average density for the atom given by equation (4); (iii) the free-atom density; and (iv) the Finnis construction optimized to the Al(111) surface with lattice constant $7.6\,a_0$.

Properties of the perfect crystal, energy minima E, the bulk modulus B and the equilibrium lattice constant a, calculated with Murnaghan's equation of state [34], are given with high precision for all four input densities, as seen in in table 2. However, for distorted bulk structures the overlapping-atom construction has been shown to do less well [9].

For the three low-index surfaces (111), (100) and (110) we have calculated the total energy and the surface energy, defined as $\gamma = \frac{1}{2}(E_{\mathrm{slab}}(n) - \frac{1}{2}E_{\mathrm{bulk}}(2n))$, where the reference bulk calculation has been made with the corresponding unit cell but with no vacuum layers. The average errors in the H functional energy for the three surfaces are 0.02 and 0.04 eV/slab for the Δn_s^* and the Finnis input densities, respectively. The result for the surface energy is even closer to the SC result.

Table 3 shows the result for Ni, obtained using the induced embedding density $\Delta n_{2.5}^*$ and the free-atom density. For $\Delta n_{2.5}^*$ the average error for the three surfaces is 0.24 eV/slab. Here the error in the fcc bulk energy for the $\Delta n_{2.5}^*$ input density is relatively large, so the resulting errors in the surface energy are below 0.1 eV/atom in all cases. This gives relative

Table 2. Total energies in eV for Al structures with lattice constant $7.75\,a_0$. Energies for induced embedding densities with $s = 2.9\ a_0$ and a mix of s for both the Hohenberg–Kohn–Sham (HKS) and Harris (H) functionals are shown as differences from the SC energies in the third column. As a comparison, the same is shown for overlapping-pseudo-atom densities and Finnis densities [7]. The bulk properties given are: equilibrium lattice constant (a), minimum energy per atom (E) and bulk modulus (B).

Al structures		Energy n^{SC}	Error in energy compared to SC result			
			$n^{\mathrm{pp\ atom}}$	n^{Finnis}	$\Delta n^{*}_{2.9}$	$\Delta n^{*\mathrm{a}}_{s}$
Free atom	E^{HKS}	−52.80	0	+ 0.04	+ 0.10	0
	E^{H}	—	0	+ 0.02	+ 0.03	0
111 slab (9 atoms)	E^{HKS}	−510.33	+ 5.64	+ 0.03	+ 0.06	+ 0.09
	E^{H}	—	−1.35	−0.05	+ 0.11	+ 0.02
γ_{111}	E^{HKS}	0.44	+ 0.94	0.00	+ 0.01	+ 0.03
	E^{H}	—	−0.20	+ 0.01	+ 0.02	0.00
Vacancy (9 − 2 atoms)	E^{HKS}	−395.49	+ 4.69	+ 0.04	+ 0.09	+ 0.72
	E^{H}	—.	−1.06	−0.03	+ 0.15	0.00
Vacancy energy	E^{HKS}	57.42	−0.48	+ 0.01	+ 0.01	+ 0.28
	E^{H}	—	+ 0.15	+ 0.01	+ 0.02	+ 0.01
Adatom (9 + 2 atoms):						
$z = 3.59\ a_0$	E^{HKS}	−622.29	+ 11.85	+ 0.53	+ 0.99	+ 1.38
	E^{H}	—	−2.11	−0.07	+ 0.14	−0.04
$z = 3.76\ a_0$	E^{HKS}	−622.42	+ 13.97	+ 0.44	+ 0.88	+ 1.13
	E^{H}	—	−2.10	−0.03	+ 0.18	−0.01
$z = 4.04\ a_0$	E^{HKS}	−622.46	+ 18.12	+ 0.31	+ 0.68	+ 1.31
	E^{H}	—	−2.10	0.00	+ 0.22	−0.02
$z = 4.37\ a_0$	E^{HKS}	−622.35	+ 22.10	+ 0.12	+ 0.28	+ 1.10
	E^{H}	—	−2.16	−0.03	+ 0.22	−0.06
$z = 5.05\ a_0$	E^{HKS}	−621.72	+ 27.05	+ 0.77	+ 0.43	+ 0.43
	E^{H}	—	−2.83	−0.16	+ 0.19	−0.05
100 slab (4 atoms)	E^{HKS}	−226.90	+ 2.83	+ 0.14	+ 0.25	+ 0.42
	E^{H}	—	−0.50	−0.05	+ 0.01	−0.04
γ_{100}	E^{HKS}	0.57	+ 1.41	+ 0.07	+ 0.12	+ 0.03
	E^{H}	—	−0.22	−0.02	0.00	+ 0.01
110 slab (4 atoms)	E^{HKS}	−226.32	2.64	+ 0.05	+ 0.12	+ 0.06
	E^{H}	—	−0.72	−0.02	+ 0.06	0.00
γ_{110}	E^{HKS}	0.84	1.32	+ 0.02	+ 0.06	+ 0.20
	E^{H}	—	−0.33	+ 0.01	+ 0.03	−0.02
a (a_0)	HKS	7.48	7.48	7.48	7.48	7.48
	H	—	7.50	7.50	7.48	7.48
E (eV)	HKS	−57.05	−57.04	−57.04	−57.04	−57.04
	H	—	−57.06	−57.05	−57.04	−57.04
B (GPa)	HKS	92.0	86.6	86.4	86.2	86.3
	H	—	86.0	84.3	85.4	87.0

[a]Superposed induced densities with neutral spheres according to table 1.

errors in the surface energy of less than 10 per cent. The bulk modulus values for both the fcc and bcc phases are seen to be significantly better for $\Delta n^{*}_{2.5}$ compared to the free-atom construction.

As a more critical test of our density construction we calculate the energy curve for an

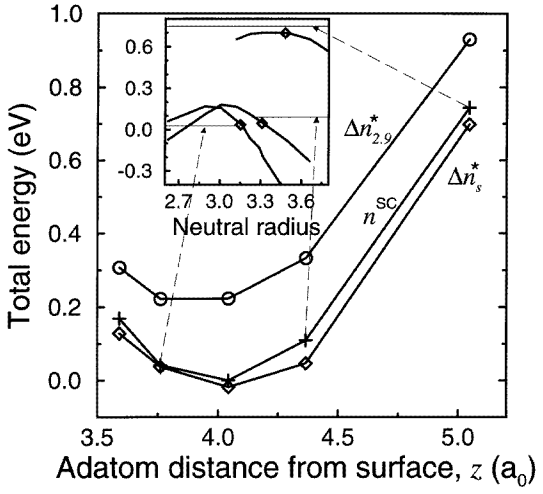

Figure 4. Total energies (relative to the SC minimum) for the Al(111) slab with an adatom at different distances from the surface. The plus signs (+) indicate the SC results, the circles (○) indicate Harris energies for $\Delta n^*_{s2.9}$ and the diamonds (◊) indicate Harris energies when the density for each atom has been chosen according to equation (4). The inset shows the total energy for variation of the adatom density for $z = 3.76\,a_0$, $4.37\,a_0$ and $5.05\,a_0$, respectively. The diamonds are the same as in the main graph. The horizontal lines indicate corresponding SC energies. The trend for the variation clearly shows the dependency on the effective coordination (i.e. the neutral radius).

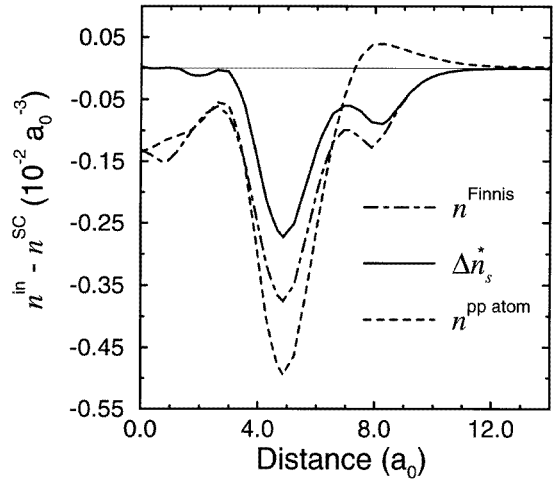

Figure 5. The error in the real-space density for the Al(111) slab. The difference between the SC density and the free-atom density, and Finnis construction, and the induced densities chosen according to equation (4), respectively, are shown for an extracted line. The line is perpendicular to the surface and stretches from the middle of the slab, through the centre–centre site, and out to the vacuum.

adatom on the Al(111) surface. Figure 4 shows the total energy for the adatom at different distances from the surface, comparing the SC result with the H functional energies for $\Delta n^*_{2.9}$ and for Δn^*_s. The agreement between the latter energies and the SC result is seen to be

Table 3. Total energies in eV for Ni structures with lattice constant $6.65\,a_0$. Results for overlapping-free-atom densities and embedding densities with $s = 2.5\ a_0$ with the Harris (H) functional are given as energy differences from the SC energies. Calculated bulk properties for Ni in the fcc and bcc structures, such as the equilibrium lattice constant (a), minimum energy per atom (E) and bulk modulus (B), are also given.

Ni Structures		Energy n^{SC}	Error in energy compared to SC result	
			$n^{\mathrm{pp\ atom}}$	$\Delta n^*_{s2.5}$
Bulk fcc (4 atoms)	E^{H}	−3842.24	−0.07	−0.17
111 slab (3 atoms)	E^{H}	−2879.95	−1.22	−0.12
γ_{111}	E^{H}	0.87	−0.58	0.00
100 slab (4 atoms)	E^{H}	−3839.89	−1.89	−0.30
γ_{100}	E^{H}	1.17	−0.91	−0.07
110 slab (4 atoms)	E^{H}	−3838.79	−2.56	−0.25
γ_{110}	E^{H}	1.72	−1.25	−0.04
Bulk fcc				
a (a_0)	H	6.56	6.58	6.54
E (eV)	H	−960.58	−960.59	−960.62
B (GPa)	H	249	218	256
Bulk bcc				
a (a_0)	H	5.22	5.23	5.20
E (eV)	H	−960.50	−960.52	−960.54
B (GPa)	H	235	197	242

very good.

The Al slab and adatom structures are expanded by 3.5% compared to the equilibrium LDA bulk values in order to enhance the differences between the $\Delta n^*_{2.9}$ and Δn^*_s densities. Table 2 shows that the Finnis construction gives better total energies compared to the $\Delta n^*_{2.9}$ density. We believe the optimization of the Finnis density to a slightly (1.6%) expanded lattice to be the reason for its better performance. Parenthetically, it can be mentioned that when comparing (as in figure 5) superimposed Finnis and $\Delta n^*_{2.9}$ densities one would actually judge the latter one as being closer to the SC density. This suggests that the Finnis procedure includes a significant optimization of error cancellations in the energy expression, along with the density optimization.

The inset of figure 4 illustrates the variational properties of the H functional. The density is varied by changing the value of the neutral-sphere radius for the adatom. Our choice for the adatom density Δn^*_s from equation (4) is seen to give results close to both the SC result and to the maximum in the H functional. The trend for variation of the adatom neutral sphere shows clearly the dependency on coordination, and thus supports our choice of embedding density given in equation (4).

The general form for the variations in the energy shown in the inset is that of a maximum. This is in agreement with equation (3) for a system dominated by the Coulomb energy. This maximum is shifted slightly (by exchange–correlation energy) relative to the SC result, giving the saddle-point behaviour expected for LDA in the general case, where both Coulomb and exchange–correlation energies are important [23].

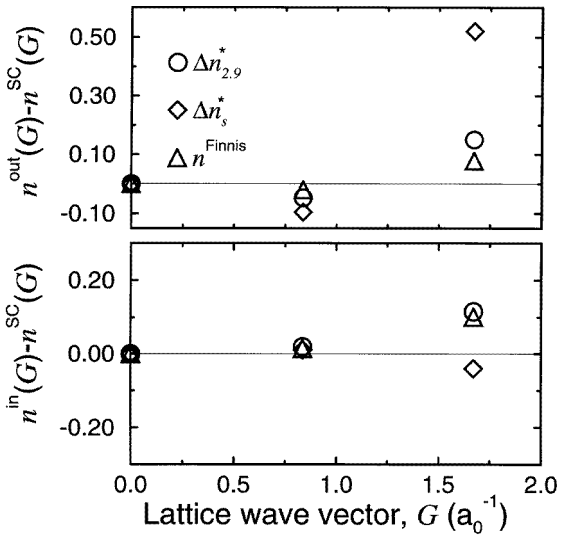

Figure 6. The error in reciprocal-space density, $n(\boldsymbol{G})/S(\boldsymbol{G})$, for the three smallest values of the reciprocal wavevectors of the Al(111) slab with an adatom placed at $z = 4.37\,a_0$. The lower panel shows the difference between input and SC densities and the upper panel shows the same for the output densities. The error in input density for Δn_s^* is in general smaller, but the sign of the errors changes for the two smallest wavevectors. This results in the large amplification of these errors found in n^{out}.

For the clean Al(111) slab, figure 5 shows the error in the real-space density in a line through the hollow site in a direction perpendicular to the surface, comparing our deviation from the SC density with those for the Finnis and for the pseudo-atom input density. The overall error for our construction is seen to be significantly smaller than for the Finnis input density. This is especially true in the bulk region of the supercell. The picture for the adatom is similar but more 'messy'. Even though the input density in real space has a overall smaller error, the HKS energy is not better for Δn_s^*. In fact, the average HKS error in table 2 is found to be bigger for this density. The error in the HKS functional is dominated by the small wavevectors $\boldsymbol{G}$, as can be seen in equation (3).

In order to investigate this more closely, we show in figure 6 the density in reciprocal space, $n(\boldsymbol{G})/S(\boldsymbol{G})$, for the Al(111) slab with the adatom at $z = 4.37\,a_0$ ($S(\boldsymbol{G})$ is the structure factor [35]). Only the three smallest wavevectors are shown for the input density and output density generated by the HKS functional. The error in input density for Δn^* is in general smaller, but the sign of the error changes for the two smallest wavevectors. This results in the large amplification of these errors found in n^{out}. In real space this implies large rearrangements of charge—so-called charge sloshing—which is a well known problem for slab calculations [31]. The Harris functional effectively removes this problem.

5. Discussion

Spherically symmetric densities for Al and Ni to be used in the Harris functional have been constructed with the physically transparent jellium model as a starting point. In agreement with Chetty *et al* [14] we find them when used as an input to the H functional to give good total-energy values for bulk and surface systems consisting of Al or Ni atoms.

Further, a systematic improvement is introduced. Following the original implementation of the effective-medium theory [20], we propose an efficient general density construction, where the average coordination number for an atom adaptively determines the embedding density used for the atom. This significantly increases the agreement between the resulting H functional energy values and the SC result. It also gives a contraction of the atom-like density that depends strongly on the average density for the atom and provides a physical way to renormalize the density.

In agreement with previous work we find H functional energies to be more accurate than the HKS ones. The error in the HKS energy is caused by the instability against density variations with such small wavevectors as are present in our surface system. The resulting charge sloshing is effectively eliminated with the H functional.

The variational properties of the H functional around the SC density constitute another important aspect for the application of the functional. For our set of densities we have found that the H functional exhibits essentially a maximum at the SC energy. Such a behaviour is expected for a system dominated by the Coulomb energy. This maximum is slightly shifted, giving a saddle-point behaviour, in agreement with the theoretical prediction, when accounting also for the exchange–correlation effects [15].

The evaluations of the H functional in this paper have been made with plane-wave programs. Several applications call for faster evaluations, however. Then it is interesting to note that input densities like ours, Finnis's and Chetty's can be used to construct the electron potential in a TB model [16]. Here the present method opens up particularly interesting perspectives with adaptive TB basis functions, an issue currently under study.

In conclusion, it should be stressed that the density construction proposed in this paper has virtues beyond earlier-published spherical-density superpositions. The increased accuracy, in particular for open systems, and the potential for an adaptive TB basis have been mentioned. In addition, it offers a description for alloys—something that is not possible with the decomposition of the density in reciprocal space [14]. A direct generalization of the jellium method to systems containing different kinds of atom is straightforward, and could provide a useful tool for constructing model potentials for alloy systems.

Acknowledgments

This work was supported by the Swedish Board for Industrial and Technical Development and the Swedish Natural Science Research Council. The use of B Hammer's (CAMP, DTU) pseudopotential plane-wave program and his assistance and the use of CASTEP are gratefully acknowledged. We have also benefited from discussions with U Engberg and L Bengtsson.

Appendix

For fits to Al embedding densities we have used

$$\frac{a + b\mathrm{e}^{-((r-c)/1.75)^2}}{\mathrm{e}^{5(r-r_c)} + 1} n^{\text{pp atom}}(r) \tag{A1}$$

and the function for Ni is

$$\frac{a + br^2(1 - c\mathrm{e}^{-((r-d)/e)^2})}{\mathrm{e}^{6(r-r_c)} + 1} n^{\text{pp atom}}(r). \tag{A2}$$

In both cases the pseudopotential atom density is exploited. The fit was made in the least-squares sense for a, b, c, d, e and r_c, with an r^2-weight on the density.

References

[1] Hohenberg P and Kohn W 1964 *Phys. Rev.* **136** B864
[2] Jones R and Gunnarsson O 1989 *Rev. Mod. Phys.* **61** 689
[3] Car R and Parinello M 1985 *Phys. Rev. Lett.* **55** 2471
[4] Harris J 1985 *Phys. Rev.* B **31** 1770
[5] Foulkes W M C and Haydock R 1989 *Phys. Rev.* B **39** 12 520
[6] Reads A J and Needs R J 1989 *J. Phys.: Condens. Matter* **1** 7565
[7] Finnis M W 1990 *J. Phys.: Condens. Matter* **2** 331
[8] Polatoglou H M and Methfessel M 1988 *Phys. Rev.* B **37** 10 403
[9] Polatoglou H M and Methfessel M 1990 *Phys. Rev.* B **41** 5898
[10] Averill F W and Painter G S 1990 *Phys. Rev.* B **41** 10 344
[11] Lin Zijing and Harris J 1992 *J. Phys.: Condens. Matter* **4** 1055
[12] Demkov A A, Ortega J, Sankey O F and Grumbach M P 1995 *Phys. Rev.* B **52** 1618
[13] Tsai M-H and Hass K C 1995 *Phys. Rev.* B **52** 16 420
[14] Chetty N, Jacobsen K W and Nørskov J K 1991 *J. Phys.: Condens. Matter* **3** 5437
[15] Robertson I J, Payne M C and Heine V 1991 *J. Phys.: Condens. Matter* **3** 8351
[16] Stokbro K, Chetty N, Jacobsen K W and Nørskov J K 1994 *Phys. Rev.* B **50** 10 727
[17] Sutton A P, Finnis M W, Pettifor D G and Ohta Y 1988 *J. Phys. C: Solid State Phys.* **21** 35
[18] Methfessel M 1995 *Phys. Rev.* B **52** 8074
[19] Puska M J, Nieminen R M and Manninen M 1981 *Phys. Rev.* B **24** 3037
[20] Jacobsen K W, Nørskov J K and Puska M J 1987 *Phys. Rev.* B **35** 7423
[21] Daw M S, Foiles S M and Baskes M I 1992 *Mater. Sci. Rep.* **9** 251
[22] Kohn W and Sham L 1965 *Phys. Rev.* **140** A1133
[23] Robertson I J and Farid B 1991 *Phys. Rev. Lett.* **66** 3265
[24] Wigner E P and Seitz F (ed) 1955 *Solid State Physics* vol 1 (New York: Academic)
[25] Ziman J M 1965 *Principles of the Theory of Solids* (Cambridge: Cambridge University Press)
[26] Almbladh C O, von Barth U, Popovic Z D and Stott M J 1976 *Phys. Rev.* B **14** 2250
[27] Hodges L, Watson R E, and Ehrenreich H 1972 *Phys. Rev.* B **5** 3953
[28] Watson R E, Herbst J F, Hodges L, Lundqvist B I and Wilkins J W 1976 *Phys. Rev.* B **13** 1463
[29] Centre for Atomic Scale Materials Physics, version of 1/30/95 (Centre for Atomic Scale Materials Physics, Denmark Technical University)
[30] Cambridge Serial Total Energy Package, version of July 1992 (Cavendish Laboratory, Cambridge University)
[31] Payne M C, Teter M P, Allan D C, Arias T A and Joannopoulos J D 1992 *Rev. Mod. Phys.* **64** 1045
[32] Bachelet G B, Hamann D R and Schlüter M 1982 *Phys. Rev.* B **26** 4199
[33] Troullier N and Martins J L 1991 *Phys. Rev.* B **43** 1993
[34] Murnaghan F D 1944 *Proc. Natl Acad. Sci., USA* **30** 244
[35] Ihm J, Zunger A and Cohen M L 1979 *J. Phys. C: Solid State Phys.* **12** 4409